JOURNAL OF GEOPHYSICAL RESEARCH, VOL. 104, NO. A2, PAGES 2343-2355, FEBRUARY 1, 1999

Fast auroral snapshot observations of bouncing ion distributions: Fieldline length measurements

M. H. Boehm and D. M. Klumpar
Lockheed Martin Advanced Technology Center, Palo Alto, CA

E. Möbius and L. M. Kistler
Space Science Center, University of New Hampshire, Durham

J. P. McFadden, C. W. Carlson and R. E. Ergun
Space Sciences Laboratory, University of California, Berkeley

Abstract. Observations of 0.01-10 keV ions at a discrete set of velocities, as expected for ions bouncing repeatedly between hemispheres, have been previously reported both at low altitudes and at geosynchronous orbit. The following two possible models of the ion source have been suggested: for the geosynchronous observations, an equatorial-acceleration model involving temporally confined ion acceleration "events" and for the low-altitude observations, a model involving a "heating wall" in the auroral acceleration region from which ions subsequently drift to other latitudes. In the latter case, the spatially bounded source appears temporally bounded from the point of view of one field line drifting over it. We report here Fast Auroral Snapshot (FAST) observations of multienergy events near local noon at several thousand kilometer altitude and show that these events orginated in a temporally localized, spatially extended, equatorial source. The dispersion pattern for individual ion bands over latitude is consistent with such a source, and not with the heating wall hypothesis, the observed energy being proportional to the square of the modeled field line length. The latter condition on the dispersion is much more precise than any imposed by a latitudinal drift model. A fit of this model to Akebono and DMSP F8 data previously published by *Hirahara et al.* (1997) is also shown. The fit to two Akebono events is accurate at lower latitudes, where the magnetic field model is expected to be reliable. The fit to DMSP data corresponding to one of the Akebono events involves additional field-aligned potentials of roughly 100 eV in the auroral zone. Observations of dispersion events of this type are expected to be useful more generally. The "nonlocal" determination of the magnetic field line length can provide a check on magnetic field models. A match of the observed field line length to the modeled one provides for greatly increased confidence in magnetic mapping.

1. Introduction

Multiple bands of ions at several energies have been observed near the equatorial edge of the auroral zone at low altitude by DE 1 and DE 2 [*Winningham et al.*, 1984; *Frahm et al.*, 1986] and by Akebono and DMSP F8 [*Hirahara et al.*, 1997]. They have also been observed at geosynchronous altitude by ATS-5 and ATS-6 [*Quinn and McIlwain*, 1979; *Quinn and Southwood*, 1982]. In the case of the low-altitude observations, it has been stated repeatedly that the observed dispersion of decreasing ion energy with decreasing latitude (not with observation time) can be explained only by convective dispersion, and not by time-of-flight dispersion along the field line [*Frahm et al.*, 1986; *Hirahara et al.*, 1997]. This model is illustrated in the Plate 1b. In this model, the ions originate in a linearly extended low-altitude source region, as an ion conic or ion beam region, and then drift perpendicularly to this source as they bounce between hemispheres. As observed on one drifting field line, the ions originate in a temporally confined ionospheric source, and the multiple narrow energy bands occur at those ion velocities which result in an integral number of bounces between hemispheres during the time interval from acceleration until observation. However, the near-equatorial observations clearly show the existence of pure time-of-flight effects, since the multiple-energy bands are observed over an extended period in one place and the dispersion patterns of individual bands are those of ion clusters bouncing back and forth across the equator [*Quinn and Southwood*, 1982]

Paper number 98JA02290.
0148-0227/99/98JA-02290$09.00

as shown in the Plate 1a. Since it appears improbable that the geosynchronous events would not also be observed at low altitudes, some reconciliation between the two interpretations is necessary. Such a reconciliation need not necessarily cover all of the events observed at lower altitudes, which span a much larger range in latitudes than the geosynchronous observations.

We begin by noting that simple time-of-flight dispersion can produce energy dispersion in latitude. Following an acceleration event which is confined in time but extended in latitude, the observed delay times are those required for the ions to repeatedly bounce between hemispheres along magnetic field lines. The bounce time is proportional to the magnetic field line length, which depends (primarily) on the magnetic latitude. A single roundtrip of a 100 eV proton at $L{\sim}10$ takes close to 3000 s, whereas a typical low-altitude satellite pass through an ion band region takes 100 to 1000 s. The satellite pass can thus often be regarded as near-instantaneous, the changes in ion energy over time (rather than latitude) during the time period of a pass being comparatively small, while the field line length variation (by a factor of >2 over ~5° in latitude) produces changes in energy of a factor 4 or more. While this effect has a spatial signature, it is quite different from the drift dispersion explanations of *Frahm et al.* [1986] and *Hirahara et al.* [1997].

We present observations form the Fast Auroral Snapshot (FAST) Explorer of multi-banded ion distributions over latitude. These tend to occur during quiet conditions, presumably because large drift velocities would complicate the signature sufficiently to make identification difficult. We show two cases in which the multiple bands (with the exception of the simultaneously observed 10 keV CPS and few eV local background distributions) show an energy dispersion over latitude which matches the square of the modeled field line length quite well. We therefore conclude that these and similar cases represent acceleration at one time over a broad range of latitudes, most probably occuring near the equator. We then consider two previously published cases of "banded ion distributions" measured by Akebono and DMSP F8 *Hirahara et al.,* [1997] and find that they also fit into this class. The *Frahm et al.* [1986] and *Hirahara et al.* [1997] drift dispersion theory can be fit to most "dispersion patterns" by assuming a corresponding drift velocity pattern; therefore it can also fit these cases, at least roughly. However, the equatorial acceleration scenario imposes more constraints on the dispersion, and still fits the data. Hence it is the more likely explanation both for the FAST cases and for those previously published by Hirahara et al..

2. Instruments

FAST ion instrumentation consists of two top-hat ion electrostatic analyzers (IESAs) similar to a standard electron top-hat analyzer [*Carlson and McFadden,* 1998] and the Time-of-flight Energy Angle Mass Spectrograph (TEAMS), essentially a top-hat with a time-of-flight section added at the end. Each IESA entrance aperture covers half of the spin plane, whereas the TEAMS entrance aperture covers a full plane perpendicular to the spin plane. In the auroral zone, the magnetic field is typically within 5°-10° of the spin plane. The IESA therefore provides essentially full pitch angle coverage at all times. TEAMS pitch angle coverage varies over a spin, from full 0°-180° coverage (twice per spin) to 90°-only coverage $\frac{1}{4}$ spin later. TEAMS is used primarily to separate H^+, He^{++}, He^+, and O^+. We show only H^+ and O^+ in this paper; the He^+ and He^{++} fluxes were too small to exclude the possibility that they represented crosstalk from other masses. For present purposes, obtaining maximal counting statistics in a certain angular acceptance range will be important. In general, the IESA provides slightly better counting statistics when fluxes are summed over angles. However, since the energy of a given peak may vary slightly with pitch angle, and since the TEAMS instrument sensitivity averaged over a spin period is concentrated at near-90° pitch angles (where the maximum fluxes typically also occur), TEAMS often provides the more useful dispersion plots for these events. TEAMS also provides confirmation of the expected dispersion delays for O^+ versus H^+.

3. Observations

Plate 2a shows energy-time spectrograms for one of the most extended FAST multiple-band ion dispersion events, including both the IESA and TEAMS (protons and oxygen) data integrated over angle. The superimposed dashed lines represent the modeled dispersion assuming instantaneous equatorial (i.e., at a point halfway to the opposite hemisphere) acceleration of ions at all invariant latitudes, occuring simultaneously at 0435:30 UT. Each dashed line represents a set of ions having bounced between hemispheres a certain number of times, specifically making [0.25, 0.75, 1.25, 1.75, 2.25, 3.25, 4.25, 5.25] (except that the IESA panel does not show 5.25 and the O^+ panel does not show 4.25 and 5.25) roundtrips. The model energy was calculated using the actual particle path length between adiabatic reflection points, including gyromotion, for an equatorial pitch angle resulting in reflection at 1.3 times the magnetic field at FAST. (These details make only a minimal difference in the curves, since the particles are nearly field-aligned for most of their path; reflection at 1.3 times the FAST magnetic field represents an average ion pitch angle of ~30° from perpendicular at FAST.) The dotted line corresponds to 0.5 roundtrips and requires some additional physics in the model: either acceleration near the opposite ionosphere or the effects of an electrostatic potential. (Although there is some evidence of a ~0.5 roundtrip population in both of the FAST events presented here, this is not true of all such events.) The corresponding magnetic field lines used in calculating the particle path length, as defined by the Tsyganenko 96 model, are shown Figure 1a. The

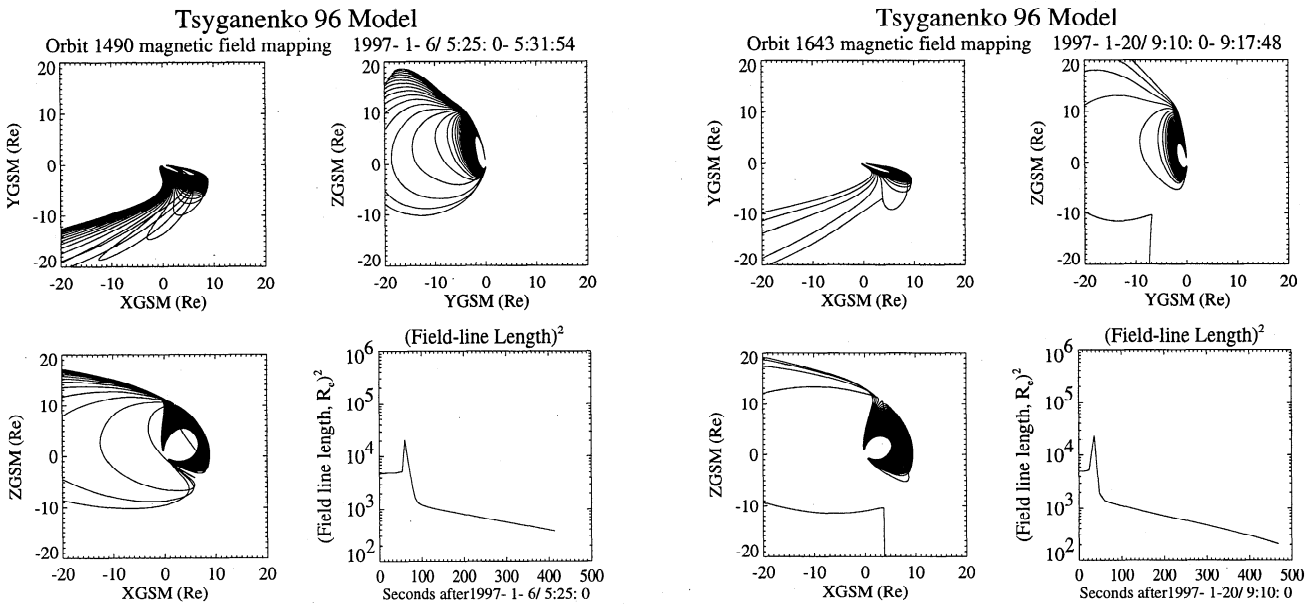

Figure 1. The magnetic field lines given by the Tsyganenko 96 model corresponding to the fitted sections of Plates 1a and 1b respectively, shown in GSM coordinates. The fourth plot in each case shows the field line length squared, in R_E^2. Field lines which do not close in these views simply reached a limit on the region to be modeled, as declared in the Tsyganenko modeling program; they may be open or they may just extend outside the reliable modeling region.

few long field lines going tailward for which both ends are shown correspond to the rapid upturn in the field line length towards larger ILAT (earlier UT); those field lines which do not appear to close (only one end of the field line shown) extend beyond the valid Tsyganenko modeling region and the corresponding field line lengths (at $<\sim$50 s) are only lower limits. The model calculation is described further below.

Figure 2 shows the proton energy distribution at 60°-120° obtained from TEAMS at 0527-0528 UT, the time of the "cleanest" distribution with the maximal number of bands. The plus signs represent the data, while the solid line shows the values of the fitted function calculated at the measurement energies. This fit assumes that the ions were accelerated at the equator, primarily toward FAST, with low-energy ions also accelerated in the opposite direction (third-lowest energy peak, at 50 eV, in Figure 2). Additionally, one peak is added corresponding to the dotted line in Plate 2a (this population is not evident in all events, and not at later times in this one); these ions may just traverse the whole field line length once. This is the fitted peak at the second-lowest energy. All together, the travel distances were assumed to be [0.25, 0.50, 0.75, 1.25, 2.25, 3.25, 4.25, 5.25] times the full-bounce (north-south-north) distance along the field line on which the satellite is located (the 1.75 line is marginally visible at later times in Plate 2, but not in Figure 2). The highest-energy fitted peak is a CPS population which does not show the dispersion; it was included to avoid distorting the fit to the dispersive peak below it. A set of multipliers involving only whole numbers [1,2,...n], or whole numbers plus one-half ([0.5,1.5,2.5...n+1/2]), as would be expected from ionospheric acceleration, does not fit the data as well, in either Figure 2 or Plates 2a and 2b. The bottom three

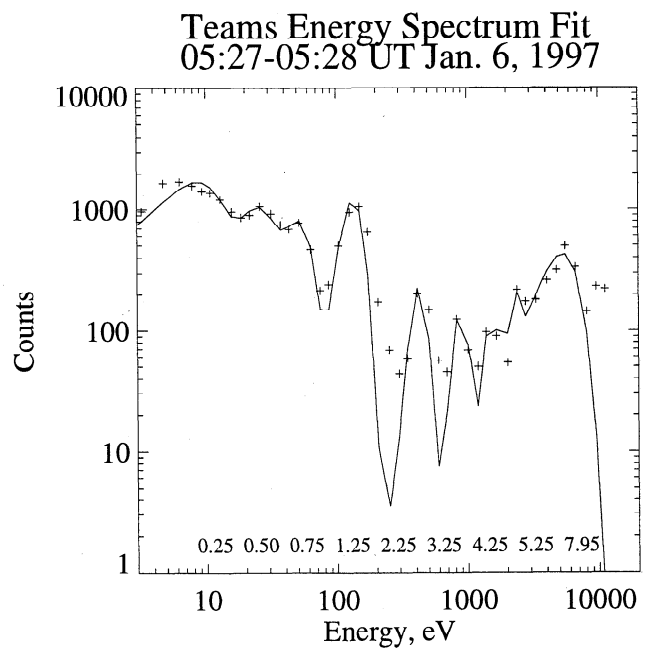

Figure 2. A TEAMS energy spectrum for orbit 1490. The fitted peaks, excepting the one at the highest energy, are at energies= $E_0 \times (0.25, 0.5, 0.75, 1.25, 2.25, 3.25, 4.25, 5.25)^2 + 3$ eV. Attempted fits with only the squares of whole numbers (as required by acceleration in the nearby ionosphere) resulted in larger errors and/or more missing numbers.

lines might fit a [1,2,3] pattern well, but then higher integers would not fit well or be missing intermittently.

The measured velocities are given by the particle path length (including gyromotion, assuming 60° pitch angle at the measurement altitude) divided by the time since the acceleration event. This time, or alternatively an overall energy multiplier, was chosen by trying different event times until good fits were obtained in Plate 2 and Figure 2. Offset energies in the range of a few eV to a few tens of eV were also added to the measurement energy in attempts to improve the fit; these allow for spacecraft potentials or a field-aligned potential close to the spacecraft. For Figure 2, during this process, a set of amplitudes (fluxes) was fitted analytically at each iteration. An offset of 3 eV was used in the final fit in Plate 2a and Figure 2 (-4 eV in Plate 2b, 20 eV in Plate 3). All peaks in Figure 2 were fitted as Gaussians in energy, as there is no detailed acceleration model which would define the shape of the individual peaks. (The widths of all the Gaussians were defined by a single linear function of the inverse velocities at the centers of the Gaussians.) The fit to the ~10 eV peak is very much dependent on the offset and the time of the fit; nonetheless, such a peak corresponding to direct propagation of the ions from the equatorial acceleration point invariably appears in the events studied so far.

A second FAST ion spectrogram is shown in Plate 2b, again with model dispersion curves superposed. An acceleration event time of 0846:30 was assumed, together with a set of distances equal to twice the particle path length along the field line times [0.25, 0.55 (dotted), 0.75, 1.25, 1.75, 2.75, 3.75]. The corresponding Tsyganenko 96 field lines, used in calculating the particle path length per bounce, are shown in Figure 1b. Here the 0.55 can again to be interpreted as corresponding to ions accelerated in the sourthern hemisphere, perhaps with a slight delay, traversing the field line fully once. It can also be explained by a moderate negative electric potential in the opposite hemisphere, causing the ions to travel faster than their measured energy would indicate for much of their trajectory. Such a potential would have small effects on the higher energies, for which there is some indication in the next two higher energies.

The direct temporal effect of changing time-of-flight delays over the ~5 min of the pass was included in the modeling in Plates 2a and 2b but contributes only a ~25% energy change over 5 min in Plate 2b and less in Plate 2a. The field line length effect contributes a factor of ~5. These are the first two cases for which such fits were done; the only prior selection is according to the number of visible bands, the length of time over which the bands are visible, and the smooth appearance of the bands.

3.1. Akebono and DMSP Data

In order to provide further checks on the equatorial source explanation of the multienergy dispersive ion events, fits were attempted for two such events in Akebono data previously published by *Hirahara et al.* [1997]. These events occurred at night, while the FAST events occurred during daytime. The data in numeric form were provided by Hirahara, allowing the generation of the data plots with superimposed fits shown in Plate 3. The fitting procedure employed is similar to that used for the FAST data, except that the direct time-of-flight changes during the period of measurement play a greater role. The assumed event times are 0643:50 and 0305:30 UT respectively, and the ions are assumed to be protons (assuming oxygen leads to worse fit; the composition was not measured directly). The assumed number of roundtrips were [0.25, 0.75, 1.25, 1.75, 2.25, 2.75] and [0.25, 1.25, 2.25, 3.25, 4.25, 5.25] for the left and right parts of Plate 3, respectively. Significant mismatches of the fit and the data occur in two places: in Plate 3a before 0652 UT, and at the lowest energy in Plate 3b. The decrease in ion energy near 0320 UT in the latter is accompanied by a simultaneous increase in the energy of precipitating electrons [*Hirahara et al.*, 1997]; the low-energy variations in Plate 3b are clearly related to field-aligned potentials. The errors of a factor of ~1.6 in velocity around 0648 UT in Plate 3a, which are consistent across multiple energies, are most straightforwardly explainable as errors in the nightside portion of the magnetic field model (the field line lengths involved are 20-30 R_E) but could also be related to a variation in the acceleration altitude, or to non-simultaneous acceleration over latitude, i.e., to a finite Alfvén propagation time of the acceleration fields, of the order of the 6 min interval between the ion acceleration and the observations. A lateral postacceleration drift over a surface-mapped distance of ~150 km in 5 min (toward higher latitudes) might also explain the discrepancy. Whatever the explanation for the discrepancy, it should be emphasized that the fit to the simple equatorial event model is good at the lower latitudes, where the field line length is known most accurately, where the equatorial Alfvén velocity as mapped to Akebono altitude is likely to be highest (producing a simultaneous acceleration event over latitude), and where electric potentials are likely to be smaller.

Plate 4 shows DMSP data for the same event as shown in Plate 3b. This data was also shown by *Hirahara et al.* [1997]. The top two panels are partially overlapping in time with Plate 3b but show measurements near 600 km altitude in the southern hemisphere. The superimposed dotted lines model [0.75, 1.25, 1.75., 2.75, 3.75, 4.75] roundtrips of protons originating halfway along the field line, for the same assumed event time (0305:30 UT) as in Plate 3b. (The curve at 1.25 roundtrips in the southern hemisphere, representing acceleration toward the southern hemisphere, is not necessarily expected from comparison with Plate 3b, but these data are separated by 2 hours in local time from the data in Plate 3b). These curves show significant errors at the lower energies; the measured energy

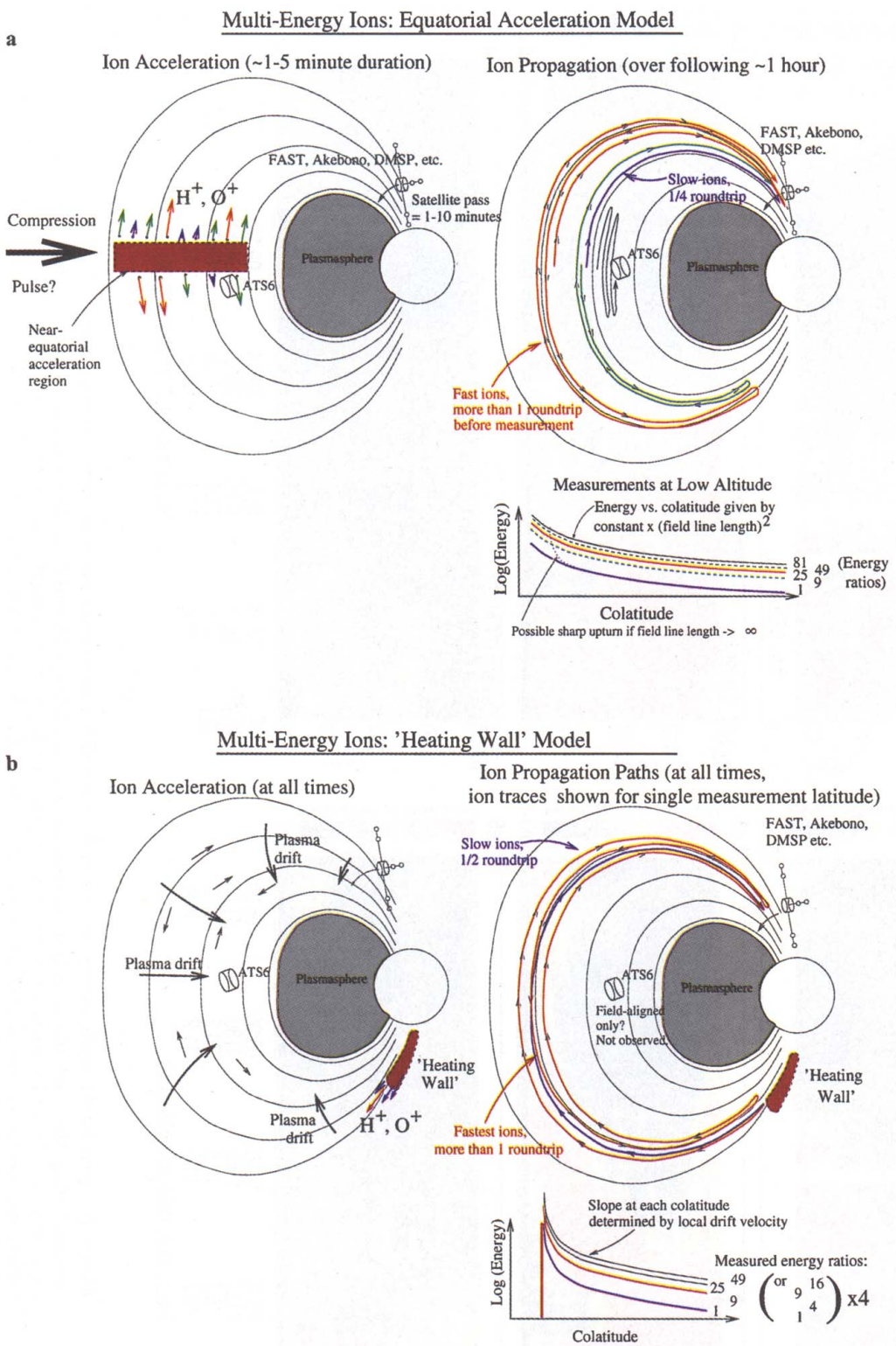

Plate 1. The two alternative explanations for the observed multienergy ion distributions. (a) In the equatorial acceleration model, ions are accelerated nearly simultaneously over a large range of L -values, to a broad range of energies. Between the acceleration time and the measurement time, each ion must make an integer+$\frac{1}{2}$ number of (unidirectional) traversals between adiabatic reflection points. This provides for discrete energy bands at the measurement point; ions having made a certain number of roundtrips will be measured only at a velocity proportional to the number of trips, and proportional to the inverse time since the acceleration event. (b) In the "heating wall" model, each ion must make an odd (if acceleration and measurement take place in different hemispheres) or even number of unidirectional traversals during the time it takes for the field line to drift from the acceleration region to the measurement point. Ions are assumed to be heated continuously in a narrow spatial region in this case. Red, green, and blue color coding is in order of decreasing energy in both cases.

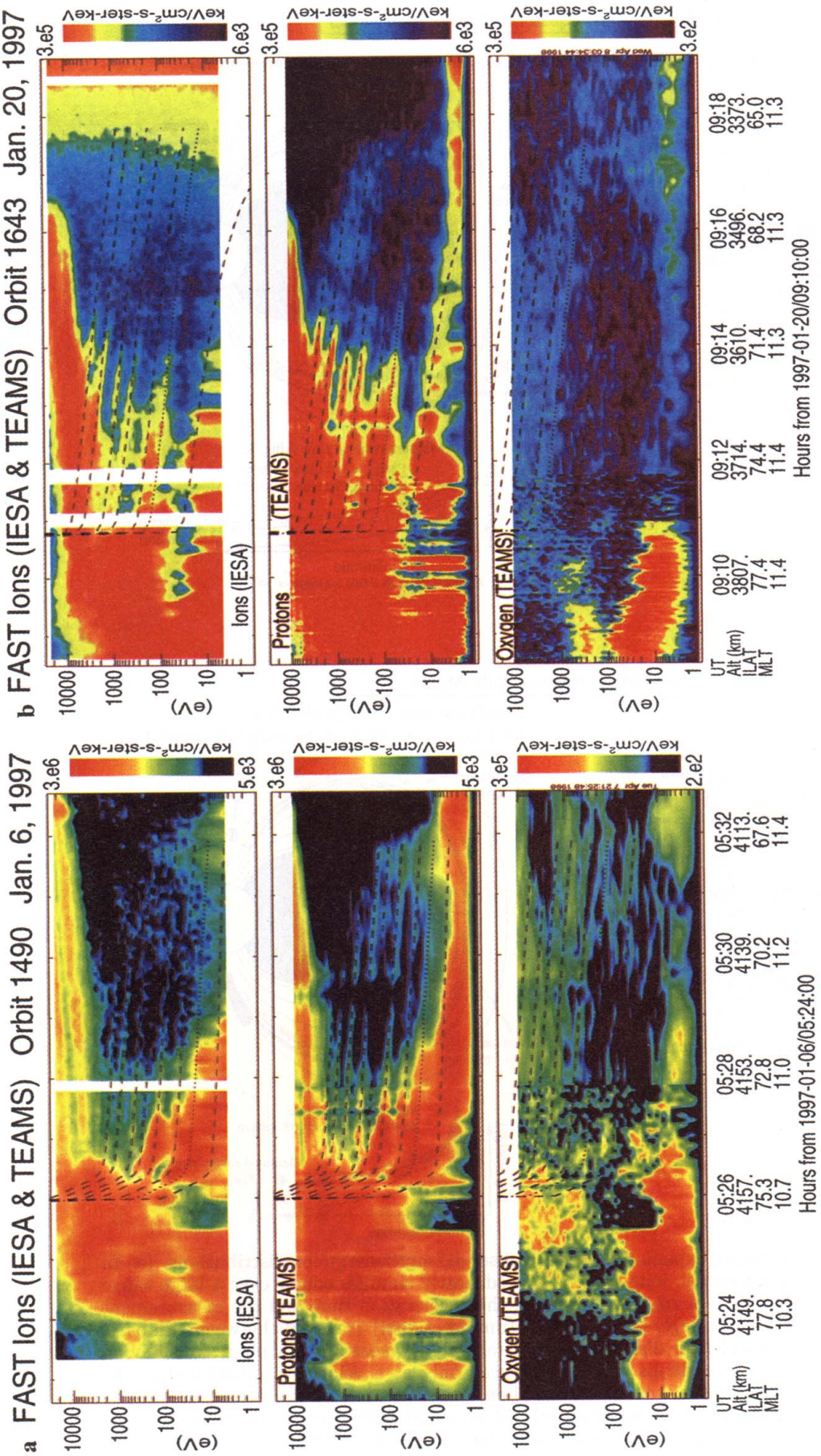

Plate 2. Two FAST multienergy ion events; (top) IESA-measured ion differential energy flux averaged over the spin plane (equal weighting over a plane containing all pitch angles). The superimposed dashed lines show the expected proton "dispersion", largely due to field line length variations, assuming simultaneous acceleration near the equator for all invariant latitudes at 0527:30 and 0846:30 UT for (a) orbit 1490 and (b) orbit 1643, respectively. The next two panels show the TEAMS spectrograms (all angles, equally weighted over the full sphere) for H^+ and O^+. A small oxygen flux is marginally visible at energies roughly equal to 16 times the proton energies. The time resolution of TEAMS is 20 s after 0528 UT in Plate 2a and 10 s after 0912 UT in Plate 2b. The data have been smoothed; counting statistics produce most of the small-scale variations in the oxygen.

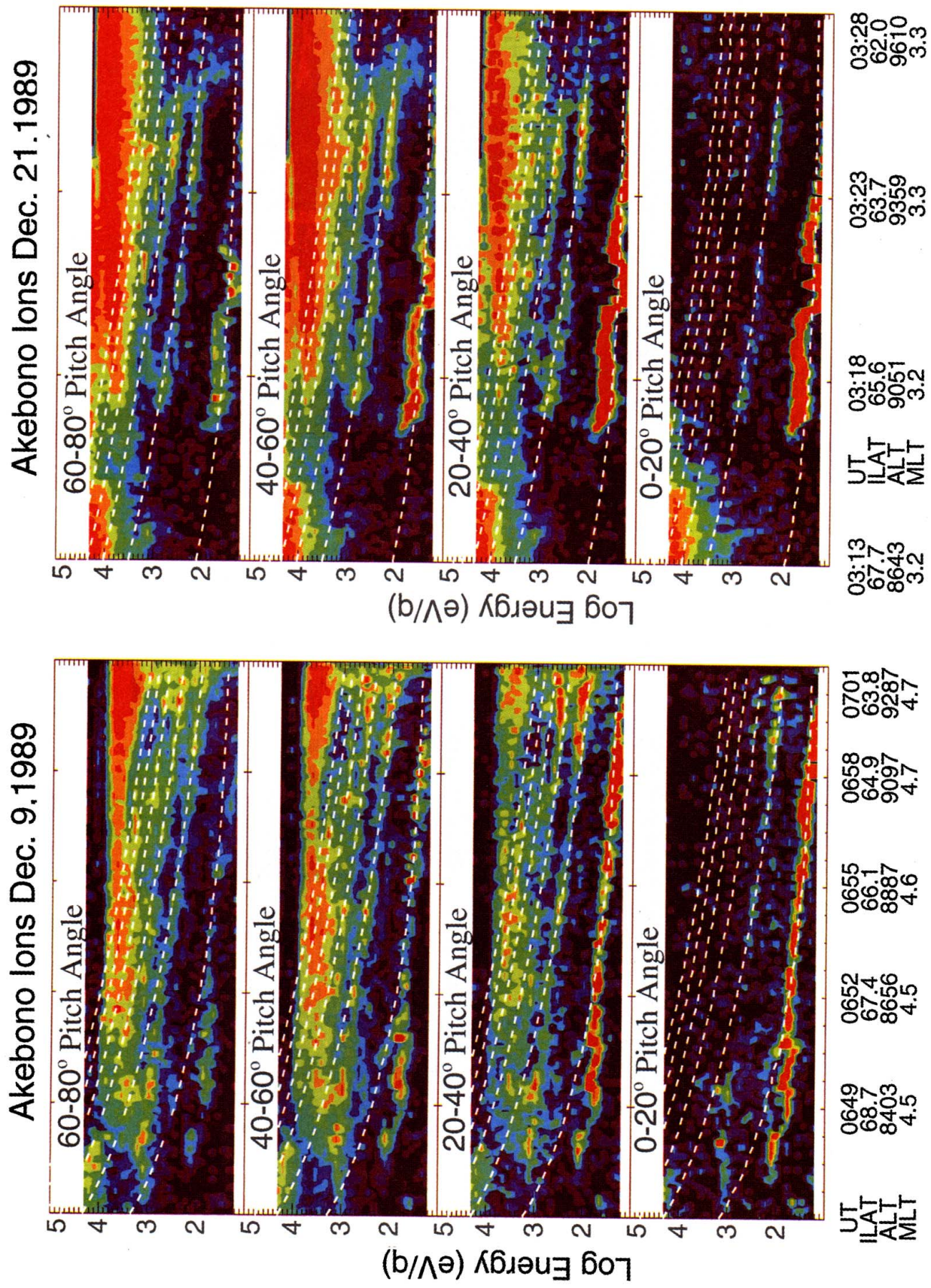

Plate 3. Two Akebono postmidnight multienergy events, taken from *Hirahara et al.* [1997]. The superimposed dashed lines again represent a model assuming instantaneous acceleration at the equator.

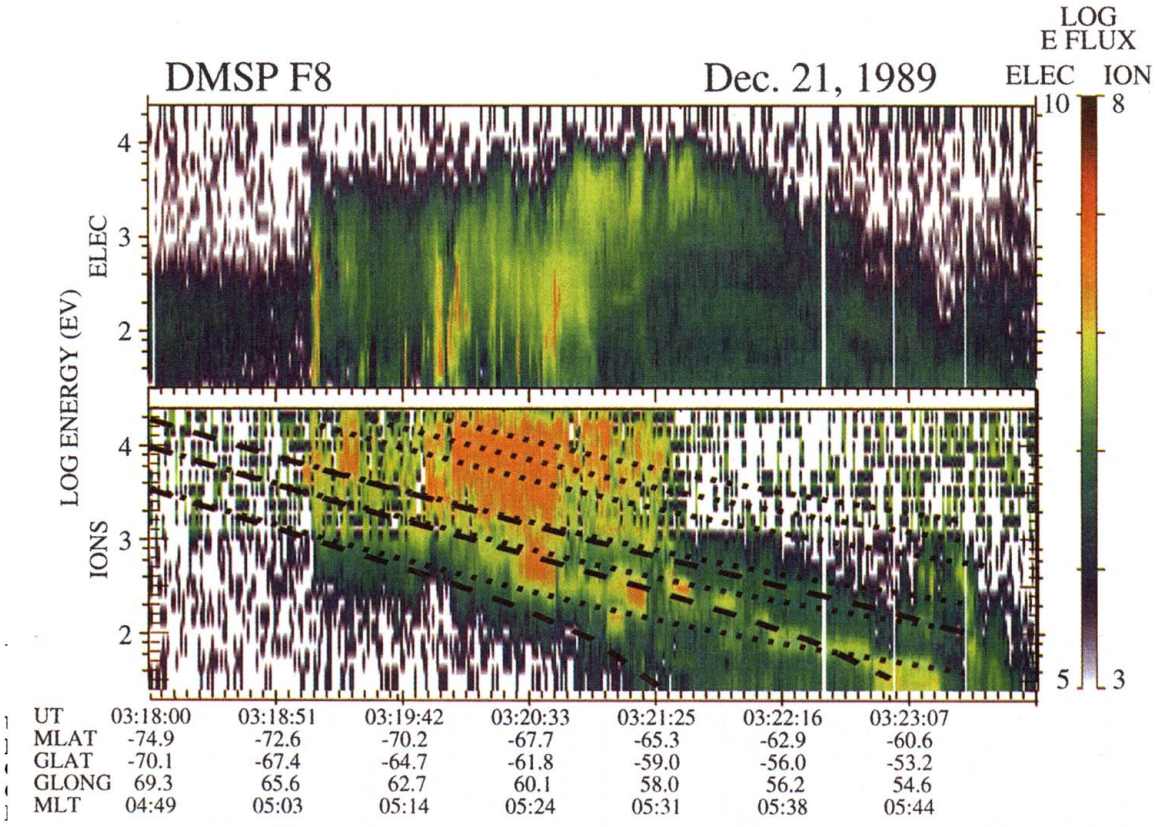

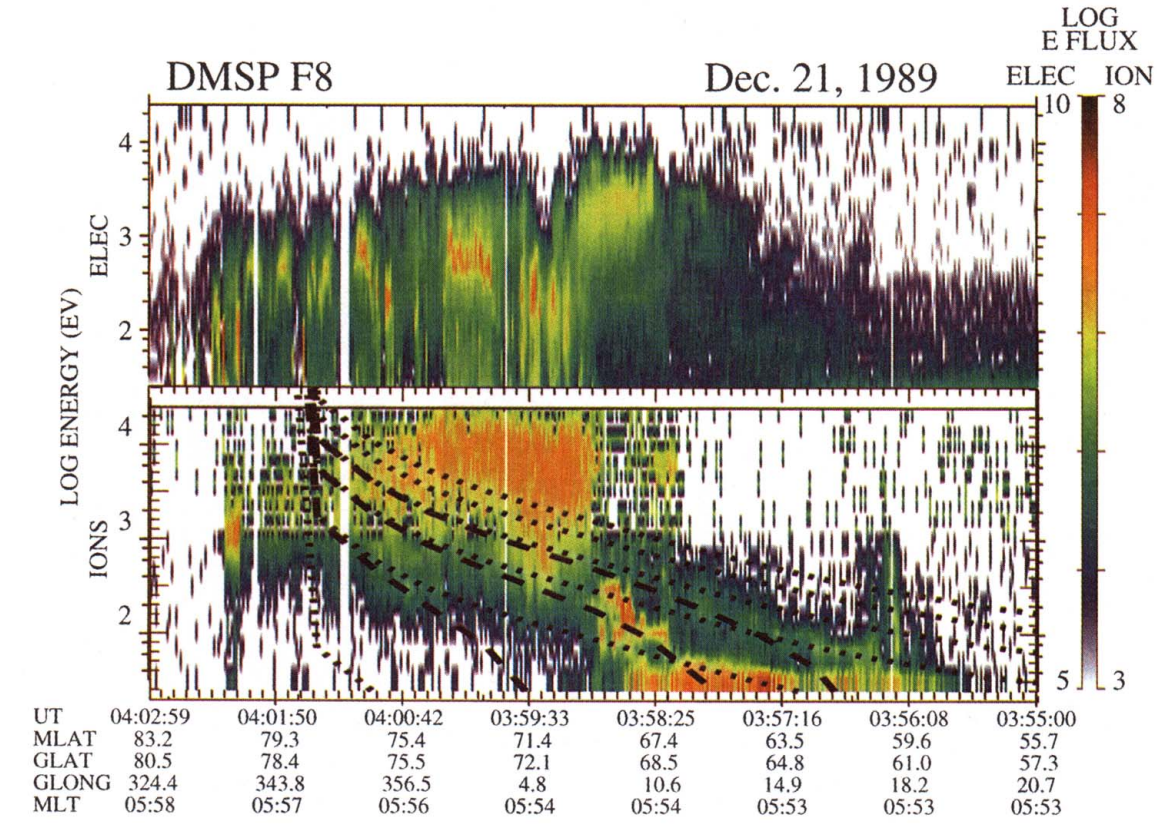

Plate 4. DMSP F8 data for the second Akebono event on December 21, also taken from *Hirahara et al.* [1997]. The first pass on the top is in the southern hemisphere and partially overlaps the time of Figure 2b. The bottom panel is in the northern hemisphere, roughly 50 min after the acceleration event. The overlaid curves use the same event time as those in Figure 2b, but in both passes, assume the existence of a $\sim$+100 V potential close to the observation point. Note the backward UT scale on the bottom.

versus time shape of the ion bands does not fit a simple dispersion curve, which flattens out at lower energies. This problem is independent of whether the dispersion mechanism involves drift, as long as no variable velocities are introduced. In order to obtain a better fit, the observed ion bands were also modeled assuming a significant (110 V) positive potential at the spacecraft (dashed lines). This could theoretically be a spacecraft potential, but probably is a low-altitude field aligned potential, as suggested by the simultaneously observed auroral electron precipitation.

The lower panels in Plate 4 show the following DMSP F8 northern pass. *Hirahara et al.* [1997] interpreted this as still representing the same acceleration event. Note that the UT timescale is backward in order to show spatial dispersion in the same sense as in Plate 4a. The superimposed dotted lines assume the same event time, and dispersion distances of [0.25,1.25,2.25,3.25,4.25,5.25] times the field line length. The fits of the dotted lines to the data, though reasonable near 1 keV, are again not particularly good overall. Assuming the same 110 V local positive potential assumed in the upper ion panel again results in better fits, shown by the dashed lines. Apparent local variations in the potential produce errors even in the dashed line fits; as expected, a smaller potential is required near 60 MLAT, at the equatorward edge of the auroral zone. The presence of variable electron precipitation is consistent with such variations in the field-aligned potential. Additional possible sources of errors in the fit exist for this nighttime auroral event: the measurement follows the assumed event time by ~50 min, during which the model assumes no field line drift; the field line mapping at the later observation times is along the flanks of the tail, reaching distances of several tens of R_E before the energy curves turn sharply upward (the model fails at this point because of field lines extending outside its assumed region of validity), hence the mapping may be inaccurate; the Alfvén propagation times over the mapped observation region may have been significant (applies mainly to the top ion panel). Nonetheless, the general slope of the ion bands near 1 keV appears to be modeled reasonably well without additional parameters. (Note that assuming a different event time for the second observation would not help, since a later acceleration time would make the dispersion flatter, given the inverted timescale.)

4. Discussion

The good fit of the multibanded energy distribution to theory in most of the above cases demonstrates that the observed ions have undergone bounce motion along the field line, with different energies corresponding to the different numbers of bounces. The *Frahm et al.* [1986] and *Hirahara et al.* [1997] drift dispersion scenario might still be applied, however. This possibility will be considered in detail first.

4.1. FAST Data: Problems With the Drift Scenario

The drift scenario would imply that the observed ions drifted from a latitude higher than the ~75° latitude of the start of the dispersive events in figure 2. The time t for an ion to reach any given observation point would be given by

$$t = \frac{\int_{acceleration\ region}^{observation\ point} \frac{1}{v_d}\, dx}{\langle v_d \rangle} = \frac{\Delta x}{\langle v_d \rangle} \qquad (1)$$

where v_d is the perpendicular plasma drift speed with respect to the acceleration region, $\langle v_d \rangle$ indicates an "average" of v_d as defined by this equation, and Δx is the integrated perpendicular distance along the drift path. v_d is assumed constant below. The observed ion velocities would be $v_i \sim n\langle D \rangle / t$ (or $v_i \sim (n+1)\langle D \rangle/(2t)$), where n is an integer and $\langle D \rangle$ is the "average" full-bounce (north-south-north) distance along the field line; i.e.,

$$\langle D \rangle = \frac{2 \int_{L_A}^{L_O} (\ D/2\ )\ dL}{L_A - L_O} \qquad (2)$$

where $D/2$ is the magnetic field line length at a given latitude, L is the latitude, L_A is the acceleration latitude, and L_O is the observation latitude. The latitudinal dependence of the ion velocity v_i is then given by $v_i = n\langle D \rangle / t \sim n\langle D \rangle v_{drift}/\Delta x$. In attempting to fit such a formula to the data assuming a constant drift velocity (and that Δx is a linear function of the observation time), with a source somewhere within ~1° of the start of the observations (such that the field lines are closed and of reasonable length), one finds invariably that the initial negative slope of the energy fit is too large over an extended latitude range, due to the dominant $1/(\Delta x)^2$ behaviour, and that in any case the second derivative is much too positive at times in the middle of the observation; such a fit cannot produce the straight line sections on the logarithmic plot.

The average slope of the dispersion in the drift scenario can only be constrained by measurements of the drift. For orbit 1490, the averaged (from 0526:30 to 0532 UT) double-probe-measured electric field perpendicular to B in the spacecraft spin plane is ~1.8 mV/m (standard deviation 2.2 mV/m at 6 s resolution) in a southwest direction, corresponding to a northwest drift. The systematic uncertainty of this field is presently estimated to be of the same order as its magnitude. The other perpendicular component of the electric field was not reliably measured due to the near-alignment of the spin plane with the magnetic field. The combination of a ~25 R_E field line length and the observed ~100 eV (~140 km/s) 1.25-bounce protons (implying ~3000 s since acceleration), decreasing in energy by 20-30% per degree latitude, would require a latitudinal ionosphere-mapped drift velocity of ~400 m/s, or a westward electric field of roughly 10 mV/m at FAST altitude. It

is unlikely that such a large field could be consistent with the measured ~2 mV/m southeast field component, even if the measurement has an uncertainty of a few mV/m. (In an oblique-arc east-west drift scenario such as that described by *Hirahara et al.* [1997], the electric field would need to be even higher.) The drift scenario therefore also appears unlikely from the point of view of the measured drifts.

4.2. Instantaneous Equatorial Acceleration Model

The equatorial single-acceleration-time model is more consistent with the observations. In generating the energy versus time lines superimposed on Plates 2a and 2b, it was assumed that drifts were small and that the acceleration took place at the equator at the same time for all latitudes. The velocities are given by the total path length of a particle making $n \pm \frac{1}{4}$ roundtrips between hemispheres along a field line passing through the observation point, divided by the difference between the assumed acceleration time and the observation time. The turning point is assumed to be at a magnetic field equal to 1.33 times that observed at FAST (i.e., 60° or 120° pitch angle at FAST, a rough average value for the pitch angle values at which particles were observed). The modeled arrival time is that at the turning point; since both downward-propagating and reflected ions are included in the FAST observations, this is an appropriate average for the expected measurement times for all the ions included in Plate 2 and Figure 2. The change in energy in an individual ion band along the satellite path is due primarily to the changing field line length, requiring a proportional ion velocity along the field line if the ion is to reach the observation point at a given time after $n \pm \frac{1}{4}$ roundtrips. A small part of the energy slope is due directly to the changing time since acceleration. An adjustment in the time of acceleration changes both the vertical position of the lines and, to a smaller extent, their slope. Given that this adjustment possibility was used to position the lines vertically, not to fit their slope, the conclusion is that the slope fits that dictated by the model. The position of the sharp upturn in energy, corresponding to a sharp upturn in the field line length given by the model, also fits well.

The assumed numbers of full bounces could possibly also be changed in discrete steps. Together with an adjustment in the event time, this would allow a change in the slope of the dispersion curves without a change in average vertical position. However, the assumed numbers of bounces between acceleration and observation - [0.25, (0.5), 0.75, 1.25, 1.75, 2.25, 3.25, 4.25, 5.25] for orbit 1490, [0.25, (.55), .75, 1.25, 1.75, 2.75, 3.75] for 1643, and [0.25, 0.75, 1.25, 1.75, 2.25, 2.75] and [0.25, 1.25, 2.25, 3.25, 4.25, 5.25] for the two Akebono events discussed, are natural ones to choose. They always include direct propagation from the source and generally include most possible numbers for two full bounces or less, differing only in the maximum energy to which ions are accelerated in each direction, and in the intermittent appearance of 0.5 bounces, possibly representing acceleration in the opposite ionosphere. Numbers ending in .25 represent acceleration towards FAST, while numbers ending in .75 represent acceleration away from FAST. Any attempt to use larger numbers of bounces to fit the data invariably results in some "missing" bands at intermediate energies. (There are also many missing numbers in a similar sequence when all ions are assumed to be accelerated upwards from one ionosphere, making n or $n + \frac{1}{2}$ of roundtrips.)

We therefore conclude that the slope in the energy-latitude dependence of the FAST dispersive ions matches that given by the equatorial-acceleration, zero-drift model, as soon as the time of acceleration is used to fit the vertical positions of the energy bands. The vertical separations of the bands fit the expectations for equatorial acceleration, resulting in $n+\frac{1}{4}$, $n+\frac{3}{4}$ roundtrips between hemispheres before observation. The energies vary over latitude as expected. Only the partial extra band at 0.5 roundtrips during orbits 1490, and the apparent centering of what should be a 0.75 roundtrip band variably between 0.5 and 0.75 during orbit 1643, require additional explanations.

Essentially the same conclusion applies to the combination of Akebono and DMSP events, although the DMSP events do not display a sufficiently clear multiband nature that they would have led to the equatorial-acceleration explanation by themselves. Significant differences in the Akebono and DMSP F8 event modeling are the following: (1) the shorter, ~10 min period from acceleration to observation (Akebono and DMSP southern pass), implying a significant direct temporal element in the dispersion effect, (2) the lack of any clear 0.5-roundtrip ion bands, simplifying the model to acceleration only at the equator in these cases, and (3) the necessity of invoking a significant, ~100 eV field-aligned potential above the spacecraft in order to explain the low-altitude DMSP dispersion pattern. In as far as difference 3 represents a complication of the model, we note that a similar complication is also required if the drift dispersion model is invoked; any simple dispersion curve involving constant velocities will flatten out at lower energies, even on a logarithmic plot. The fact that the invoked potential is positive makes this offset more or less an expected element of the model. If any of the field-aligned potentials necessary to accelerate the sharp auroral precipitation patterns (visible immediately before 0321 UT and immediately after 0359 UT) extend into the regions after 0321 and before 0359 UT, or if the slight electron maxima at ~200 eV at 0358:20-0359 UT and at 0321:00-0321:20 UT are assumed to be the result of electrostatic acceleration, then an ion-decelerating potential of the order of 100 eV is implied. Note that the characteristic energy of several keV in the plasma sheet precipitation (after 0321 and before 0359 UT) is primarily thermal; the energy distribution

in this differential energy flux plot is broad, and a keV accclcrating potential is not implied.

In calculating the superimposed dispersion curves in Plate 2 (and Plates 3 and 4), the Tsyganenko 96 model [*Tsyganenko,* 1996, available at www-spof.gsfc.nasa.gov, /pub/kolya/versail.ps; *Tsyganenko and Stern,* 1996] was used. This model requires as input *Dst*, solar wind dynamic pressure, B_y, and B_z. *Dst* data were obtained from the Kyoto data center World Wide Web page, and solar wind data were obtained from the CDAWeb and OMNIWeb. IMP 8 and Wind data, roughly time shifted by the solar wind propagation delay to the magnetosphere, were used as input to the field model for the two FAST events. The Akebono and DMSP F8 events required interpolation of solar wind data 3-7 hours separated from the event time. The effects of errors in these parameters on the lower latitudes are minimal; no major changes in activity were involved.

4.3. Acceleration Mechanism, Additional Near-Ionospheric Acceleration?

There are two energy bands in Plates 2a and 2b which require complications to the equatorial acceleration scenario. Plate 2a has a partial "extra" band at ~0.5 roundtrips, while in Plate 2b the second-lowest band appears displaced more toward low energies with increasing time, the final energy corresponding to ~0.5 roundtrips. This distance appears to imply ion acceleration near the southern ionosphere. If a compression pulse was responsible for the equatorial heating, near-ionospheric heating may have occured in the form of conic and beam formation when a shear wave component of the pulse reached the polar ionosphere after propagating along the magnetic field. The Alfvén travel time from the equator to the ionosphere would have been much shorter than the proton travel time at 20-50 eV (50-80 km/s). Alternatively, it is possible that the actual propagation distance of the ions was 0.75 roundtrips, the shorter apparent distance being due to electrostatic potentials in the opposite hemisphere which changed the energy of the ions in the middle of their trip, or reflected them before they reached the their normal southern reflection point. A small potential would have affected the lowest energies (except the 0.25-roundtrip band, since these ions were confined to the northern hemisphere). An extra band such as that in Plate 2a would be explained more easily by near-ionospheric heating, although partial reflection at a potential is also a possible explanation. The slow energy decrease relative to the 0.75-roundtrip model in Plate 2b is better explained by potentials, but such a wide band may also be interpreted as consisting of two wide bands near the energies required for 0.5 and 0.75 roundtrips. A slowly changing flux ratio could then have produced the apparent energy shift over time. We will not consider the application of these two interpretations to Plate 2 in more detail, except to consider in a broad sense whether the energy in a compression pulse capable of producing the equatorial acceleration would have been sufficient to also produce ionospheric heating and/or field-aligned potentials.

In order to arrive at some semiquantitative results, we will consider a specific acceleration scenario. Assume that the original ion distribution was flat in differential energy flux ($1/v^4$ in distribution function, where v is the ion velocity). This is suggested by the near-constancy of the observed differential energy flux over energy ranges broader than the individual bands. Also assume that a compression pulse heated this distribution adiabatically. In a dipole geometry (admittedly a rough approximation) the perpendicular energy during compression is proportional to $1/R^3$, where R is the radial distance of the ion to earth. The parallel energy (and we are concerned with ions that reach low altitudes, and hence are nearly parallel at the equator) will be proportional to $1/R^6$ in as far as the ions remain near the equator during the whole compression (ions far from the equator are accelerated less, producing the banding). These proportionalities are determined straightforwardly from the ion gradient drift (for perpendicular velocities) and curvature drift (for parallel velocities) in a dipole geometry, in combination with an azimuthal electric field. Given the observed energy band peak-to-valley flux ratios of a factor of ~5, the change in R for the ions due to compression must have been a factor ~1.3. Such a compression could be caused by a factor ~2 change in the solar wind pressure, at least near the outer end of the observations where the larger peak/valley ratios are observed. While Wind observed pressure variations of ~30% or less at the appropriate times, it was located at $[x,y,z]$= [44,-62,-8] R_E and $[x,y,z]$ = [136,-35,-16] R_E (GSM) during orbits 1490 and 1643 respectively, and hence might have missed some variations. The "compression" could also be more local, perhaps because of cusp reconnection and corresponding antisunward convection in the ionosphere ($[B_x,B_y,B_z]$= ~[4,-3,+2] nT and ~[5,1,6] nT were measured by Wind, at times equal to the event time minus the upstream distance of Wind divided by the solar wind velocity). For several reasons (the requirement that even the higher-energy ions remain near the equator during the whole compression; maintaining a clear separation between energy bands), the compression cannot have lasted longer than ~3-5 min at individual ion locations. We will assume 3 min; the corresponding velocity and equatorial electric field at 7-10 R_E from Earth (B ~ 40-100 nT) are then of the order of 50-100 km/s and 3 mV/m, or ~100 mV/m in the ionosphere if mapped statically. The Poynting flux for such a signal traveling along the magnetic field line at the equator would be of the order of 3×10^{-5} W/m^2 at the equator (assuming an Alfvén velocity of 300 km/s) or ~0.03 W/m^2 if it all propagated along field lines to the ionosphere. The latter is a reasonably large auroral energy flux (corresponding to 10 μA/m^2 at 3 kV, for

instance) which would easily be capable of significant ion heating and of generating field-aligned potential regions. Even if only a fraction of this energy flux directly reaches the poles, it is still likely to be sufficient for ion heating and potentials on the order of tens of eV.

In summary, any compressive pulse capable of producing the observed equatorial acceleration is also likely to involve a sufficient Poynting flux to heat ions and produce field-aligned potentials in the auroral acceleration region. It is not surprising that an extra band of <100 eV near-ionosphere-heated ions should appear or that there should be some distortion in the <100 eV bands due to field-aligned potentials.

4.4. Importance of Multi-Energy Dispersive Ions in Magnetospheric Dynamics

We will specifically discuss the event in Plate 2a, which has some of the highest observed ion fluxes near the beginning and fades to barely evident bands near the end. This FAST event involved number densities of 0.1 (when barely visible) - 30 cm^{-3}, maximal energy densities of $\sim$1000 eV/cm^{-3}, maximal possible energy fluxes (i.e., the energy flux of half the distribution) of a few times 10^{-9} W/cm^2, and maximal possible currents (i.e., the current of half the distribution) of $\sim 0.1 \mu A/m^2$. The largest energy and number densities are marginally significant perturbations at FAST altitude, while the currents and energy fluxes are negligible compared to typical auroral values at FAST. Whether the mapped densities, energy fluxes, or currents at the same L value near the equator are dominant is a more difficult question. If the velocity distributions were isotropic near the equator, the equatorial parameters would be essentially the same as those at low altitude, in which case (at densities up to 30 cm^{-3}) they could easily exceed typical total values of these parameters near the equator. However, *Quinn and McIlwain* [1979] indicate that most of the events on the dayside are field-aligned, with a characteristic pitch angle range of the order of 15°, implying a density at the equator $1\frac{1}{2}$ to 2 orders of magnitude lower than that measured at FAST. In this case, the equatorial density in this event varies from a maximum of $\sim$0.3-1 cm^{-3} at large L values (intense parts of the measured event, ILAT$\sim$75°) to <0.003 cm^3 (mapping to barely visible bands in FAST data), and the maximal possible equatorial current density from the ions would be $\sim 3 \times 10^{-3}$ $\mu A/m^2$. The ions in the more intense parts of the event may then still represent the full ion distribution near the equator, and even the ion currents may play a moderate role in the plasma dynamics there. The densities are thus consistent with adiabatic acceleration of the full equatorial ion population by a "convection surge" [*Quinn and Southwood,* 1982] or magnetospheric compression. This type of acceleration is dominantly parallel (in a dipole magnetic field configuration), with the final parallel energy being proportional to the initial parallel energy. The intense ion fluxes in the observation then correspond to regions of greater fractional parallel acceleration (i.e., the curvature drift carries ions through the largest electric potential in these regions), which results in small pitch angles and a large fraction of ions reaching FAST altitude.

5. Conclusions

Two FAST multiple-energy daytime ion events at the equatorward edge of the auroral zone have been shown to be due to ions bouncing between hemispheres. Each set of ions was accelerated near the equator in a single acceleration event extending over $\sim$5° of magnetic latitude. Discrepancies with the model at the lowest energies are easily explained as being due to small electrostatic potentials and to ion heating near the opposite ionosphere resulting from the compressive pulse which also heated ions at the equator. The latitude range of a single dispersive event maps to positions from near-geosynchronous to near the magnetopause on the dayside. The duration of the acceleration process is constrained by the accuracy of the fits to be of <$\sim$5 min, enough time for a compression pulse or other signal to propagate at the Alfvén velocity through the corresponding region at the equator.

The statistical determination of occurrence frequencies of these events in FAST observations is beyond the scope of this paper. The events shown are some of the best ("best" defined as having a large number of extended, nearly continous, smooth bands in the spectrogram) found within several hundred orbits of data. Marginal events do occur in a significant fraction of the orbits. These typically consist of one to three energy bands with roughly the right dispersion characteristics over a $\frac{1}{2}$ to 2 min period, at the equatorward edge of the auroral zone. The observations in Plate 2 were during quiet times; the simple dispersion signature will occur only when there is very limited plasma drift during the ion propagation period. It appears likely that similar acceleration events are common during more active times when their signatures are more complicated. These may cause a significant fraction of the ion precipitation at the equatorward edge of the auroral zone.

Two previously published nighttime multiple-energy Akebono ion events [*Hirahara et al.,* 1997] can also be modeled reasonably well using similar equatorial-acceleration event assumptions. In one case the model does not fit well at invariant latitudes above 67°. This error occurs where the model is expected to be least accurate: at nighttime, in the winter, at latitudes within the auroral zone, where variations in the tail current can produce significant variations in the field line length that cannot be taken into account by the average Tsyganenko field; where there may be significant field-aligned potentials and drifts; and where Alfvén propagation times over the source region may be significant, in particular as the fitting to this event calls for an event time

only ~5 min before the start of observations. The second Akebono event requires only small field-aligned potentials to explain the behavior of the lowest-energy ion band. Two DMSP F8 passes showing the latter event require field-aligned potentials of the order of ~100 eV between Akebono and DMSP altitudes (9000 and 600 km) in order to explain the low-energy end of the observed dispersion patterns using the Akebono event acceleration time. Such a potential would also be required in the drift dispersion theory with a reasonable drift velocity pattern. The simultaneously observed electron precipitation at DMSP provides independent evidence for the existence of field-aligned potentials during these passes (a quantitative comparison of electron acceleration potentials with the potential assumed for the ions would be difficult).

The alternate, drift dispersion model suggested by *Hirahara et al.* [1997] and *Frahm et al.* [1986] can also roughly fit the data, *if* a corresponding drift velocity pattern is assumed. Within broad limits, there is a one-to-one mapping from an arbitrary observed dispersion pattern to a latitudinal drift velocity pattern. Hence almost any observed "dispersion pattern" can fit the drift dispersion theory. However, assuming a constant drift velocity gives a worse fit to the data than that provided by the equatorial instantaneous acceleration model. Since the latter model of a field line length dependent dispersion defines a dispersion shape with only the event time as a free parameter, it is favored, in as far as it fits the data, over the drift dispersion model, which can fit most dispersion patterns. (In the case of FAST observations, electric field measurements also do not show the electric fields required by the drift dispersion model.)

The model of near-simultaneous equatorial acceleration over broad spatial regions thus appears to be applicable to many banded ion distributions. In as far as source propagation delays and potentials along the field line can be excluded, the latitudinal variation in ion band energies during these observations can provide a direct check on the field line length given by a magnetic field model. Statistical studies of field line lengths using "marginal" events may be possible without 100% certainty in the identification of individual events. We note that a series of low-altitude satellites along one orbit might well allow the measurement of the time development of field line lengths.

Acknowledgments. The authors would like to thank P. Newell and M. Hirahara for forwarding the DMSP and and Akebono data shown in this paper. Thanks also to A. Lazarus, R. Lepping, K. Ogilvie, and the Wind SWE team for providing the WWW solar wind parameter data used in the modeling. This work was supported by NASA under grant number NAG5-3596.

The Editor thanks J.-E. Wahlund and another referee for their assistance in evaluating this paper.

References

Carlson, C. W., and J. P. McFadden, Design and application of imaging plasma instruments, in *Measurement Techniques in Space Plasmas: Particles, Geophys. Monogr. Ser.,*, vol. 102, edited by R. F. Pfaff, J. E. Borovsky, and D. T. Young, p. 125, AGU, Washington, D. C., 1998.

Frahm, R. A., P. H. Reiff, J. D. Winningham, and J. L. Burch, Banded ion morphology: Main and recovery phases, in *Ion Acceleration in the Magnetosphere and Ionosphere, Geophys. Monogr. Ser.,* vol. 38, edited by T. Chang, p. 98, AGU, Washington, D. C., 1986.

Heelis, R. A., J. D. Winningham, W. B. Hanson, and J. L. Burch, The relationship between high-altitude convection reversals and the energetic particle morphology observed by atmosphere explorer, *J. Geophys. Res., 85*, 3315-3324, 1980.

Hirahara, M., T. Mukai, E. Sagawa, N. Kaya, and H. Hayakawa, Multiple energy-dispersed ion precipitations in the low-latitude auroral oval: Evidence of E×B drift effect and upward flowing ion contribution, *J. Geophys. Res., 102*, 2513-2530, 1997.

Quinn, J. M., and C. E. McIlwain, Bouncing ion clusters in the Earth's magnetosphere, *J. Geophys. Res., 84*, 7365-7370, 1979.

Quinn, J. M., and D. J. Southwood, Observations of parallel ion energization in the equatorial region, *J. Geophys. Res., 87*, 10,536-10,540, 1982.

Tsyganenko, N. A., Effects of solar wind conditions of the global magnetospheric configuration as deduced from data-based field models, in *Proceedings of the Third International Conference on Substorms (ICS-3), Eur. Space Agency Spec. Publ., ESA SP-389*, 181-185, 1996.

Tsyganenko, N. A., and D. P. Stern, Modeling the global magnetic field of the large-scale Birkeland current systems, *J. Geophys. Res., 101*, 27,187-27,198, 1996.

Winningham, J. D., J. L. Burch, and R. A. Frahm, Bands of ions and angular V's: A conjugate manifestation of ionospheric ion acceleration, *J. Geophys. Res., 89*, 1749-1754, 1984.

M. H. Boehm and D. M. Klumpar, Lockheed Martin Advanced Technology Center, Palo Alto, CA 94304. (boehm@europa.spasci.com)

C. W. Carlson, R. E. Ergun, and J. P. McFadden, Space Sciences Laboratory, University of California, Berkeley, CA 94720.

L. M. Kistler and E. Möbius, Space Science Center, University of New Hampshire, Durham, NH 08324.

(Received April 20,1998; revised June 26, 1998; accepted June 26, 1998.)